ACS OMEGA

http://pubs.acs.org/journal/acsodf

Article

Studies on Synthesis, Characterization, and Photocatalytic Activity of TiO_2 and Cr-Doped TiO_2 for the Degradation of *p*-Chlorophenol

Md. Kamrul Hossain, Md. Mufazzal Hossain, and Shamim Akhtar*

Cite This: *ACS Omega* 2023, 8, 1979−1988

Read Online

ACCESS | Metrics & More | Article Recommendations | Supporting Information

ABSTRACT: TiO_2 and Cr−TiO_2 nanoparticles (NPs) have been synthesized by the sol−gel method using titanium isopropoxide as the precursor of Titania. The prepared samples were analyzed by employing scanning electron microscopy, energy-dispersive X-ray spectroscopy, X-ray diffraction, X-ray photoelectron spectroscopy, and Fourier transform infrared analyses. Under UV irradiation, the photocatalytic activities of TiO_2 and Cr−TiO_2 were observed by estimating the % degradation of *p*-chlorophenol (PCP) as a sample pollutant. The extent of degradation was investigated, varying the catalyst dosage, initial PCP concentration, irradiation time, and solution pH. The experimental results show that efficiency of catalysts initially increases but decreases later on, whereas the % degradation of PCP is the highest at its lowest initial concentration. For TiO_2 and Cr−TiO_2 NPs at their optimal catalyst dosage of 2.0 g/L, acidic pH, and with UV irradiation for 90 min, the observed % degradation of PCP is 50.23 ± 3.12 and 66.51 ± 2.14%, respectively. Thus, the prepared Cr−TiO_2 NPs have enhanced the degradation efficiency of PCP with an irradiation time which is four time less than those reported earlier. From the kinetics analysis, the degradation reaction of PCP is found to follow a pseudo-first-order model and the rate constants are 0.0075 and 0.0122 min^{-1} for pure TiO_2 and Cr−TiO_2 NPs, respectively. The present study has further revealed that owing to the lower rate of electron−hole pair recombination, the photocatalytic activity of Cr−TiO_2 NPs becomes higher than that of TiO_2. Therefore, as viable photocatalytic agents, Cr−TiO_2 NPs are suggested to be used also for efficient degradation of other organic pollutants.

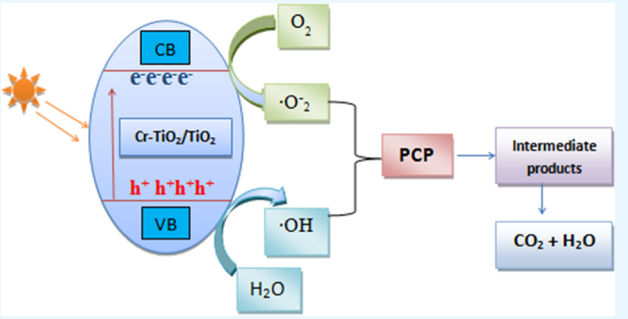

INTRODUCTION

Chlorophenols are highly toxic and non-biodegradable compounds used in various industrial processes as in the synthesizing dyes, paints, pesticides, paper, pulp, wood preservatives, and pharmaceuticals.[1,2] It is found to irritate the eyes, throat, skin, and nose, causes coughing, wheezing, and raises other respiratory issues due to its poisonous and corrosive properties.[3] Moreover, long-term exposure causes headache, tiredness, anxiety, liver and renal problems, paresis, nausea, and eventually coma and death.[4,5] That is why they are identified as a priority hazardous pollutant by the US Environmental Protection Agency and European Commission decision 2455/2001/EC.[6] Therefore, the removal of isomeric chlorophenols from the environment, particularly from the contaminated waters, is of utmost importance.

For the removal of such toxic pollutants from wastewater, recently, several methods such as adsorption,[7] photodegradation,[6] biodegradation,[8] and advanced oxidation processes (AOPs)[4,9] were developed. Among these methods, AOPs are considered as the most effective ones for the total degradation of organic pollutants.[10,11] AOPs work with the generation of highly reactive hydroxyl radicals, which can react with almost all classes of organic pollutants, leading to their total or nearly complete mineralization, or formation of more unstable intermediates. The complete oxidation leads to mineralization generally prone to yield CO_2 and H_2O.

Various semiconducting oxides, such as titanium dioxide (TiO_2), ZnO, CeO_2, CdS, Fe_2O_3, CuO, WO_3, Bi_2WO_6 metal−organic frameworks, and graphene oxide (GO)−chitosan hydrogel, are used as photocatalysts for different purposes like environment, energy, solar cells, electrolysis, and chemical synthesis.[12−17] Among all these semiconducting oxides, TiO_2 is largely used due to its non-toxicity, affordable cost, chemical stability, photonic activity, and low environmental impact.[18] However, despite all these benefits, as TiO_2 has a wide band gap (3.2 eV), its photocatalytic efficiency is less in removing pollutants under different light sources. Therefore, to enhance the photocatalytic activity of TiO_2, researchers employed different processes like metal doping such as Ag, Mn, Cu, V, Mo, Cr, Fe, and Zn[18−24] and non-metal doping such as P, C,

Received: August 9, 2022
Accepted: December 16, 2022
Published: January 3, 2023

N, S,[25−28] and TiO_2 nanocomposites.[29] Numerous studies have found that doping metal oxides with transition metals can improve the photocatalytic activity, owing to a shift in the absorption region from UV to visible light due to a change in their electronic structure.[30] Cr^{3+} is considered an ideal metal for doping TiO_2 among the various transition metals due to its compatible radius, which is very close to the radius of Ti^{4+}; that is why, Cr^{3+} can easily be incorporated into the TiO_2 lattice.[31] Inturi et al.[32] evaluated the photocatalytic activity of TiO_2 nanoparticles (NPs) doped with Fe, Cr, V, Mo, Mn, Ce, Cu, Co, Y, Ni, and Zr. Their findings show that Cr, Fe, and V have more impressive catalytic activity than other transition metals (Mn, Mo, Ce, Co, Cu, Ni, Y, and Zr).

To prepare TiO_2 and doped TiO_2, researchers[33−38] have employed various techniques such as sol−gel, hydrothermal, chemical vapor deposition, solvothermal, and wet impregnation. Of the above methods, the sol−gel process appears to be the most straightforward and sophisticated one,[39] with several advantages, including better control over the growth of NPs, lower processing temperature, higher purity, shorter processing time, precise composition control, better homogeneity, and lower cost.[40,41] In addition, the sol−gel method provides fine spherical NPs of uniform size. Therefore, it has been widely utilized to prepare TiO_2 and Cr-doped TiO_2 nanomaterials, usually starting with acid-catalyzed hydrolysis of titanium(IV) alkoxides.[42] Representing R as an alkyl group, the following reactions can describe the method:

Hydrolysis

$$\mathrm{Ti(OR)_4} + n\mathrm{H_2O} \rightarrow \mathrm{Ti}(OR)_{4-n}(\mathrm{OH})_n + n\mathrm{ROH} \quad (1)$$

Condensation

$$\mathrm{Ti-OH} + \mathrm{OR-Ti} \rightarrow \mathrm{Ti-O-Ti} + \mathrm{ROH} \quad (2)$$

$$\mathrm{Ti-OH} + \mathrm{OH-Ti} \rightarrow \mathrm{Ti-O-Ti} + \mathrm{H_2O} \quad (3)$$

The present investigation synthesized TiO_2 and Cr-doped TiO_2 using the sol−gel method. The prepared NPs were characterized using different instruments in scanning electron microscopy (SEM), energy-dispersive X-ray spectroscopy (EDS), X-ray diffraction (XRD), and X-ray photoelectron spectroscopy (XPS) techniques. To establish the optimum degradation conditions under UV light sources, the photocatalytic degradation of *p*-chlorophenol (PCP) was investigated under different experimental conditions, such as catalyst loading, initial PCP concentration, irradiation time, and solution pH. The kinetics of all these photocatalytic degradation reactions was also investigated, evaluated, and compared.

EXPERIMENTAL SECTION

Materials. Titanium isopropoxide (TTIP) ($C_{12}H_{28}O_4Ti$) used as the titanium precursor, chromium nitrate [$Cr(NO_3)_3 \cdot 9H_2O$, Merck] as the source of chromium, ethanol (CH_3CH_2OH), nitric acid (HNO_3), and deionized water were used for the synthesis of TiO_2 and Cr-doped TiO_2. The PCP (Sigma-Aldrich) was used as a model organic pollutant for the photocatalytic tests. All the chemicals were used without further purification.

Synthesis Procedure. 50 mL of 1.0 M TTIP solution was prepared using ethanol as the solvent. At room temperature, this TTIP solution was added drop by drop to 460 mL of deionized water, stirred vigorously for 1 h, and by adding nitric acid, the pH of the solution was maintained at 2.0. To get the doping of Cr, an appropriate amount of solution of $Cr(NO_3)_3$ was added to the mixture and stirred. The prepared sol was heated at 60 °C to evaporate the remaining water and then dried at 100 °C for 6 h to obtain the gels. The powders were then calcined at 400 °C for 6 h. The undoped TiO_2 was synthesized following the same process but without using any doping agent (chromium nitrate).

Characterization of Synthesized Samples. A scanning electron microscope (FE-SEM S-4500, HITACHI Ltd. Japan) was used to examine the morphology of the prepared samples of NPs. To characterize the crystalline phase and size of the TiO_2 and Cr-doped TiO_2 powders, an X-ray diffractometer (Ultima IV, Rigaku Corp., Japan) with Cu Kα radiation (λ = 0.154056 nm) was employed at room temperature. The EDS (FE-SEM EDX S-782XII, HORIBA Ltd., Japan) was used to analyze the element content of catalysts. To investigate the composition and valence state of the elements of prepared NPs, an XPS PHI 5000 VersaProbe II (ULVAC-PHI INC.) technique was implemented. Finally, to analyze the NP samples further, the Fourier transform infrared (FTIR) spectra were recorded by using a FTIR spectrophotometer (IRPrestige-21, Shimadzu, Japan).

Photodegradation of PCP. The photocatalytic activity of the synthesized TiO_2 and Cr-doped TiO_2 NPs was studied by irradiating the suspension with an UV lamp (λ = 254 nm) all inside a closed lamp house. Firstly, an appropriate amount of the catalyst was taken in a beaker with 20 mL of deionized water and put in an ultrasonic cleaner for 30 min. Next, a requisite amount of PCP solution containing the catalyst suspension was taken in a beaker, kept in the dark for about 30 min with constant stirring to reach the adsorption−desorption equilibrium, and then all were irradiated by UV radiation for up to 90 min. The suspensions at different time intervals were collected in test tubes, and to get their clear solutions, each of the suspensions was centrifuged at a constant speed for nearly 30 min. Then, absorbance of the solutions was measured with the help of an UV−vis spectrophotometer (UV-1800, Shimadzu, Japan). Eventually, the % degradation of PCP was evaluated from the measured absorbance by the following equation

$$\%\ \text{degradation} = [(A_o - A)/A_o] \times 100\% \quad (4)$$

Here, A_o represents the initial absorbance of PCP, and A is the absorbance measured at a particular irradiation time, t. The UV−vis spectra for the photodegradation of PCP irradiated at different time intervals using the Cr−TiO_2 as the catalyst are shown in Figure S1.

RESULTS AND DISCUSSION

Characterization. *Scanning Electron Microscopy.* To investigate the surface morphology and shape of the synthesized NPs of TiO_2 and Cr-doped TiO_2, SEM studies were carried out. Figure 1 displays the relevant SEM images for TiO_2 and Cr−TiO_2 samples. It has been observed that all the samples are in the form of agglomerates of sphere-like-shaped NPs.[43] The SEM images have also revealed that doping does not change the topology of the catalyst surfaces, and all the particles are relatively uniform in size[44] for the Cr-doped TiO_2, as shown in Figure 1b.

Energy-Dispersive Spectroscopy (EDS) Analysis. The elemental analysis for Cr−TiO_2 was performed by employing the EDS. As Figure 2 exhibits, the EDS spectra confirm the presence of Cr, Ti, and O in the Cr-doped TiO_2. Furthermore,

https://doi.org/10.1021/acsomega.2c05107
ACS Omega 2023, 8, 1979−1988

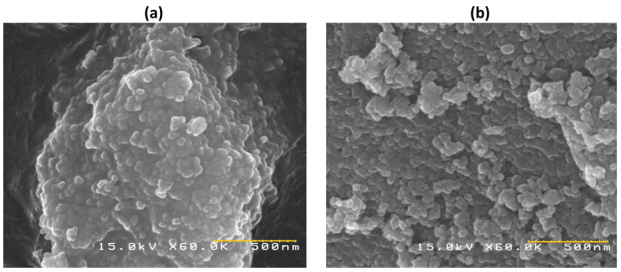

Figure 1. SEM images of nanomaterials: (a) pure TiO_2 and (b) Cr−TiO_2.

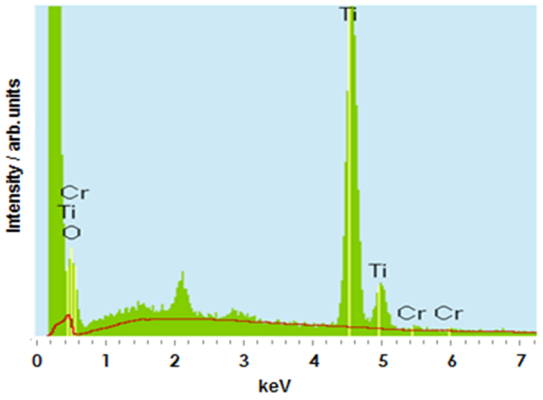

Figure 2. EDS spectra of the prepared Cr−TiO_2 NPs.

the percent weight of Ti, O, and Cr in the prepared Cr-doped TiO_2 is found to be 45.06, 54.40, and 0.54%, respectively. The images in Figure S2a−c exhibit the atomic distributions of Cr, O, and Ti, respectively, in the Cr-doped TiO_2 sample. (d) EDX image of Cr−TiO_2.

XRD Analysis. Figure 3a shows the XRD patterns of the TiO_2 and Cr-doped TiO_2 NPs. The samples were measured in the range from 2θ = 20 to 80°. The observed diffraction peaks for pure TiO_2 and Cr−TiO_2 originated at 25.3, 37.9, 48.1, 53.98, 55.1, 62.7, 68.8, 70.36, and 75.10°, which are indexed as (101), (004), (200), (105), (211), (204), (116), (220), and (215), respectively. These peaks are an attributive indication of the anatase phase of TiO_2 and Cr−TiO_2, and they also coincide well with the standard JCPDS card no. 21-1272. The XRD patterns of NPs prepared using the sol−gel method also matched those reported earlier and confirmed their anatase phase.[43−46] On the other hand, the Cr-doped TiO_2 NPs show an anatase phase with no characteristic peak of Cr, which implies that Cr^{3+} ions are incorporated into the lattice of TiO_2,[47] promoting a decrease of oxygen vacancies similar to that reported by others.[48,49] By using the Debye−Scherrer equation, the average crystalline size, D, of the prepared samples was calculated as follows

$$D = \frac{k\lambda}{\beta \cos\theta} \tag{5}$$

where λ is the wavelength of the X-ray beam used, β represents the peak width of the half-maximum, θ is the Bragg diffraction angle, and k is the Scherrer constant. The particle sizes of pure TiO_2 and Cr-doped TiO_2 NPs were found to be 26.97 and 24.33 nm, respectively. It is also observed that compared to pure TiO_2 sample, the particle size of the Cr−TiO_2 sample decreases because of the introduction of Cr into the lattice of

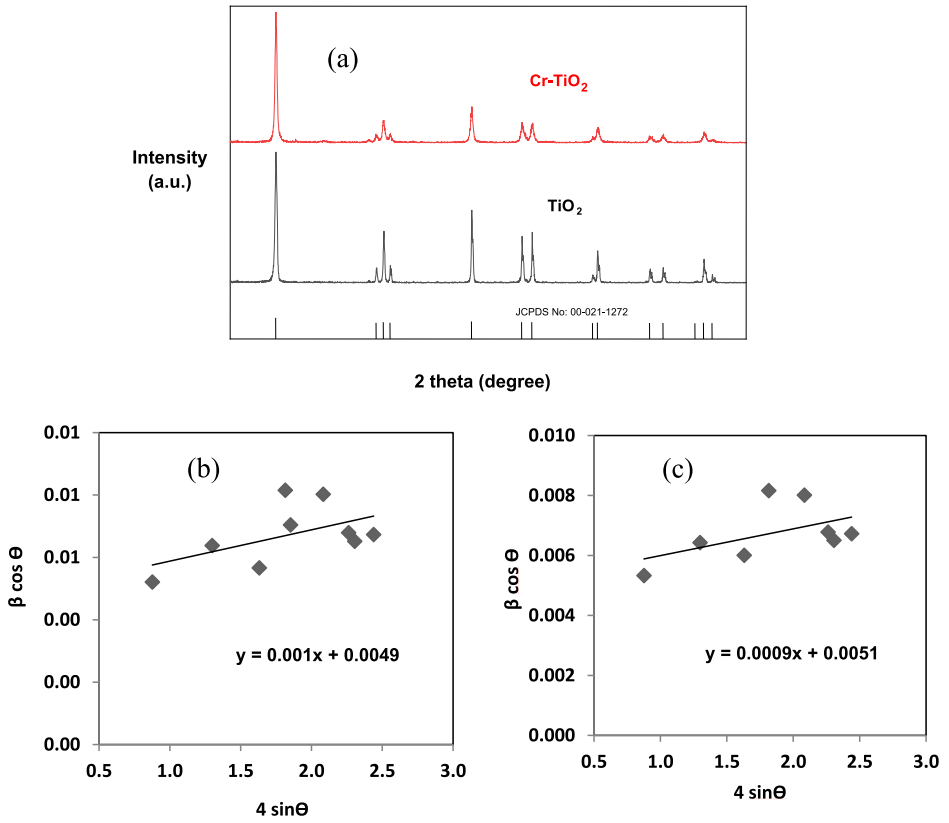

Figure 3. (a) XRD pattern(s) of pure TiO_2 and Cr-doped TiO_2 NPs. Williamson−Hall (W−H) plots for (b) pure TiO_2 and (c) Cr-doped TiO_2.

https://doi.org/10.1021/acsomega.2c05107
ACS Omega 2023, 8, 1979−1988

Table 1. Lattice Parameters and Crystallite Sizes of the Synthesized Samples

sample	$a = b$ (Å)	C (Å)	$V = a \times b \times c$ (Å^3)	strain $\times 10^4$	crystallite size (W–H plot) (nm)	crystallite size (D–S eq) (nm)
TiO_2	3.78	9.40	134.31	10	28.30	26.97
Cr–TiO_2	3.78	9.55	136.45	9	27.19	24.33

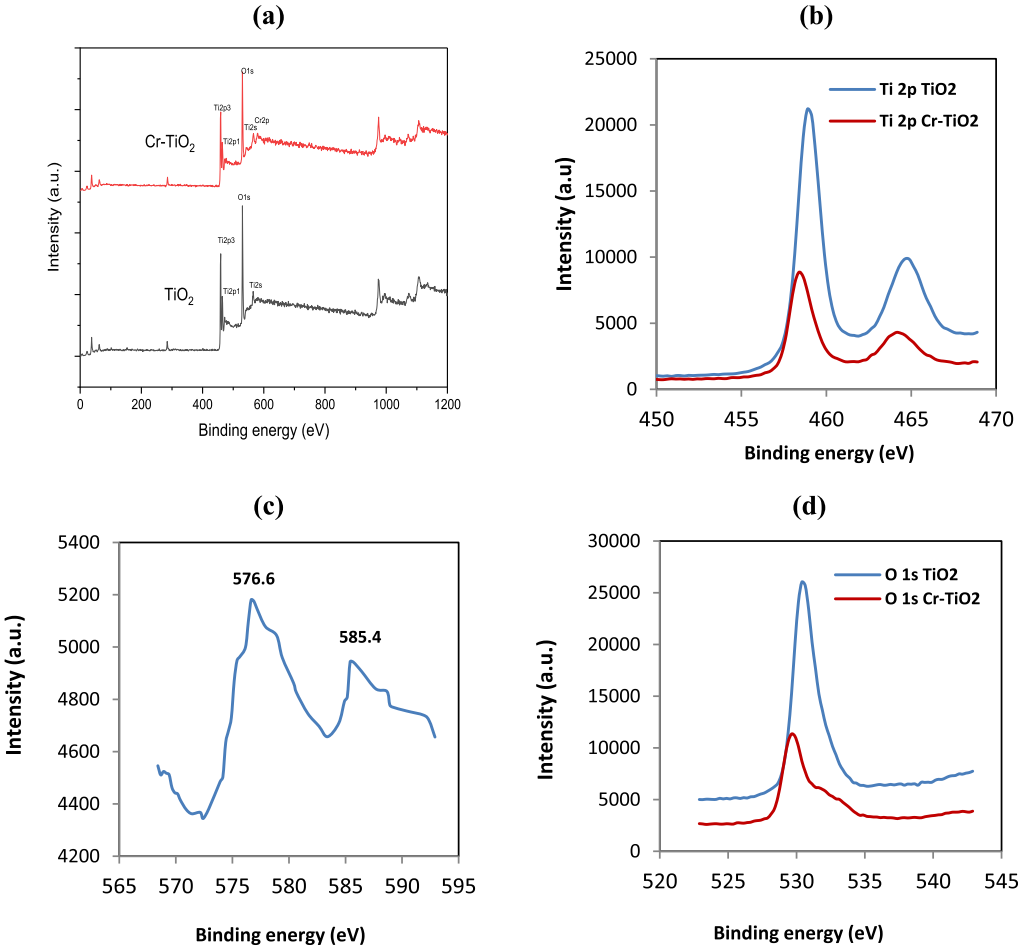

Figure 4. XPS spectra of TiO_2 and Cr–TiO_2: (a) survey spectra, (b) Ti 2p, (c) Cr 2p, and (d) O 1s.

TiO_2.[47] The lattice parameters for the (200) and (101) peak positions were calculated by using eq 6

$$\frac{1}{d^2} = \frac{h^2 + k^2}{a^2} + \frac{l^2}{c^2} \tag{6}$$

where h, k, and l are the Miller indices, and d represents the interplanar distance. The calculated data are summarized in Table 1, where the "a" values are the same for both samples, but "c" varied slightly, resulting into the difference in their cell volumes, V. However, the ionic radius of Cr^{3+} (0.63 A) is very close to that of Ti^{4+} (0.68 A), so that, substitutional doping may occur without any significant change in their unit cells.[50]

The lattice strains of the nanomaterials of TiO_2 and Cr-doped TiO_2 were calculated using the Williamson–Hall (W–H) plot method.

$$\beta \cos\theta = \epsilon(4 \sin\theta) + \frac{0.9\lambda}{D} \tag{7}$$

where λ is the wavelength of X-ray radiation, β represents fwhm, θ is the Bragg angle of the diffraction peak, D is the crystalline size, and ϵ is the lattice strain parameter. The linear fitting plots of $\beta \cos\theta$ against 4 $\sin\theta$ are shown in Figure 3b,c. From their slopes, the calculated lattice strain parameters for TiO_2 and Cr–TiO_2 are obtained as 10.0×10^{-4} and 9.0×10^{-4}, respectively. Lattice strain measures the distribution of lattice constants arising from crystal imperfections, such as lattice dislocation. Crystalline size and lattice strain contribute to the broadening of the peak. Lattice micro-strain is a combined effect of crystal defects, mechanical deformation, and chemical composition of NPs. The lattice strain values are very close to each other for the pure TiO_2 and Cr-doped TiO_2 which suggests being due to the close ionic radii of both Cr^{3+} and Ti^{4+}.

XPS Analysis. The surface composition and chemical state of the elements in TiO_2 and Cr–TiO_2 were determined by employing the XPS analysis. The main elements Ti and O for TiO_2 NPs and Ti, O, and Cr in Cr-doped TiO_2 NPs were observed from their survey spectrum, as shown in Figure 4a. The binding energies of Ti $2p_{3/2}$ and Ti $2p_{1/2}$ were located at 464.6 and 458.9 eV, respectively, for TiO_2 and at 463.6 and 457.9 eV, respectively for Cr–TiO_2 (Figure 4b). In both cases, difference of 5.7 eV between the peaks of Ti $2p_{3/2}$ and Ti $2p_{1/2}$ indicates that Ti is in the form of Ti^{4+}.[51,52] As Figure 4 (c) exhibits, the two 2p peaks in the XPS spectra of Cr at 576.6

https://doi.org/10.1021/acsomega.2c05107
ACS Omega 2023, 8, 1979–1988

and 585.4 eV can be assigned to that for the Cr^{3+} $2p_{3/2}$ and Cr^{3+} $2p_{1/2}$, respectively, which are also clearly indicating that Cr element is present as Cr^{3+} in the Cr−TiO_2.[53−55] For O, a high-resolution spectrum is shown in Figure 4d. The characteristic O 1s peaks for TiO_2 and $CrTiO_2$ located at 530.6 and 529.15 eV, fitted by two components at 529.4 and 531.3 eV, may be ascribed as due to the lattice oxygen of TiO_2 (O_L) and the surface hydroxyl oxygen (O_{OH}) in TiO_2, respectively.[56,57] Additionally, the O 1s peak in Cr−TiO_2 has slightly shifted toward the binding energies lower than that of pure TiO_2. This is most likely due to the existence of oxygen vacancies resulting from the Cr doping in TiO_2.[58]

FTIR Analysis. The FTIR spectra of NPs are shown in Figure S3. FTIR spectra were recorded in the solid phase using the KBr pellet method in the wavenumber range, 4000−400 cm^{-1}. The surface OH group's stretching and bending vibrations are attributed to the peaks at 3442 and 1630 cm^{-1}, respectively.[44] The peaks observed in the region 400−900 cm^{-1} were assigned to the Ti−O stretching and O−Ti−O flexion vibrations, respectively.[53] The intensity of corresponding peaks for Cr−TiO_2 is higher than that of the undoped TiO_2. The broadening of the bands of Cr−TiO_2 confirms the presence of defects which arises due to oxygen vacancies existing in the system for the incorporation of Cr into the TiO_2 lattice.[53]

Photocatalytic Activity of TiO_2 and Cr−TiO_2. *Effect of Catalyst Dosage.* Figure 5 shows the effect of catalyst dosage

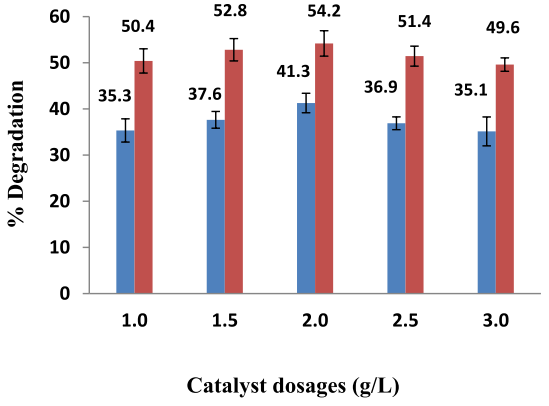

Figure 5. Effect of catalyst dosages on the % degradation of PCP at $[PCP]_0 = 2.0 \times 10^{-4}$ M, irradiation time = 90 min, and pH = 6 (blue bar: solid TiO_2; brown bar: solid Cr−TiO_2).

on the photodegradation of PCP, varying the amount of TiO_2 and Cr−TiO_2 catalysts from 1.0 to 3.0 g/L at the initial concentration of PCP as 2.0×10^{-4} M and irradiation time t = 90 min. Figure S4 shows the change in absorbance during the photodegradation of PCP at different dosages of TiO_2 and Cr−TiO_2 as the catalysts. In cases of pure TiO_2 and Cr-doped TiO_2, the observed % degradation of PCP is found to increase with increasing catalyst dosage up to 2.0 g/L and reached their maximum values as 41.28 ± 2.11 and 54.19 ± 2.75%, respectively. This could be attributed as due to an enhancement in the accessible surface area of the photocatalysts, enabling the formation of more active radicals.[59,60] However, with the further increment in the catalyst dosage from 2.5 to 3.0 g/L, the degradation efficiency decreased gradually. At the increased catalyst loading, this lowering of the degradation rate can be attributed as due to the deactivation of activated molecules through collisions with the Titania ground state molecules,[61] lack of light penetration, and the cumulative photocatalytic effects in the solution.[62] Earlier, from their investigation on the effect of the catalyst loading, Venkatachalam et al.[63] reported that, 2.0 g/L is the optimal catalyst dose for the photodegradation of PCP. This is also in support of our present finding.

Effect of the Initial Concentration of PCP. The effect of its initial concentration on the degradation of PCP was investigated by setting the concentration of the experimental samples between $[PCP]_0 = 1.0 \times 10^{-4}$ and 2.5×10^{-4} M and fixing the catalyst dosage at its optimal value, 2.0 g/L, as shown in Figure 6. The change of absorbance during the photo-

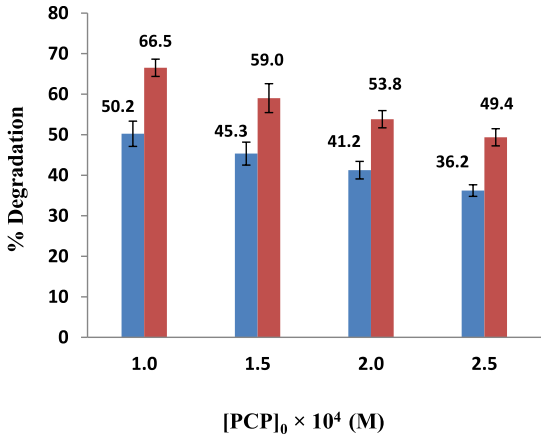

Figure 6. Effect of the initial concentration of PCP on its % degradation maintaining the catalyst loading = 2.0 g/L, irradiation time = 90 min, and pH = 6 (blue box solid TiO_2 and brown box solid Cr−TiO_2).

degradation of PCP at its different initial concentrations using TiO_2 and Cr−TiO_2 as catalysts are exhibited in Figure S5. It has been observed that, when $[PCP]_0$ is increased the degradation efficiency declines. The highest and lowest % degradations were found at $[PCP]_0 = 1.0 \times 10^{-4}$ and 2.5×10^{-4} M, respectively. At the lowest concentration of PCP, that is, at 1.0×10^{-4} M, the % degradation of PCP were 50.23 ± 3.12 and 66.51 ± 2.14% for pure TiO_2 and Cr−TiO_2, respectively. Here, the effect of free radicals on the aromatic ring is suggested to influence degradation efficiency the most; the efficiency starts to decline as the initial concentration of PCP is raised and ultimately the lowest % degradation value is reached at its highest concentration.[64] These findings have revealed that at higher concentrations the number of hydroxyl radicals produced in the reaction medium and on the catalyst surfaces goes to be limited.[65] Additionally, as the substrate concentration rises, intermediates may be formed and adsorbed on the surfaces of catalysts. Eventually, at higher concentrations of PCP the slow diffusion of these intermediates from the catalyst surfaces can deactivate the active sites of the photocatalyst, resulting into the so-called decreased degradation efficiency.[66]

Effect of Solution pH. The pH dependence of the degradation rate of the sample containing PCP concentration as 2.0×10^{-4} M and TiO_2 suspension as 2.0 g/L within pH = 2.0−9.0 is displayed in Figure 7. The % degradation of PCP is found to decrease as the initial pH of solution increases. This leads to suggest that in highly acidic pH values, the overall degradation occurs more favorably and, hence, with enhanced effectiveness. The explanation is given as follows. Below the

https://doi.org/10.1021/acsomega.2c05107
ACS Omega 2023, 8, 1979−1988

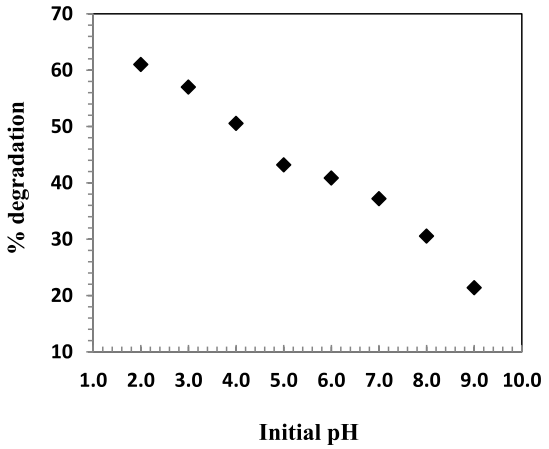

Figure 7. Effect of initial pH on the % degradation PCP, at $[PCP]_0$ = 2.0×10^{-4} M, TiO_2 dose = 2.0 g/L, and irradiation time = 90 min.

zero-point charge pH (pH_{zpc}), which is 6.25 for TiO_2, the surfaces of TiO_2 NPs are likely to be positively charged; conversely, the chlorophenol and its intermediates are mostly negative and neutral. Hence, adsorption of PCP on the surface of TiO_2 would be favored at lower pH, and therefore, the degradation reaction would become faster. Moreover, in the mechanism of TiO_2-mediated photodegradation, when the pH is greater than pH_{zpc}, the formation of HO_2 and $^{\bullet}OH$ free radicals becomes quite slow.[67] In the present investigation, the maximum % degradation of PCP is found to be 61.02% at pH = 2.0; gradually decreases with the increment of pH, and ultimately, it goes down to as low as 21.41% at pH = 9.0.

Table 2 displays the photocatalytic activities of TiO_2 and other doped-TiO_2 NPs for the degradation of PCP under different conditions. The data here reveal that compared to the catalytic activity of the previously reported samples, the percent degradation of PCP is quite high when our prepared NPs of Cr-doped TiO_2 are used as photocatalysts. Therefore, due to their excellent photocatalytic activities, these Cr−TiO_2 NPs can also be used for efficient photodegradation of other pollutants like PCP.

Degradation of PCP in Absence of Catalyst, Irradiation, or Both. The degradation strategy of the PCP in the absence of the catalyst, irradiation, or in absence of both the catalyst and irradiation was also investigated. The results are represented as in Figure S6. Under each of the above experimental conditions, degradation of PCP is not found to occur. Hence, the degradation reaction of PCP has been suggested to occur exclusively aided by the irradiation and photocatalyst all together. This is also highly consistent with our present findings.

Kinetics Study. To investigate the kinetics of photocatalytic degradation of PCP, a pseudo-first-order model is used. The integrated form of the equation follows as

$$\ln(C_0/C_t) = kt \tag{8}$$

where C_0 is the initial concentration, C_t is the concentration at time t, and k is the apparent rate constant. Figure 8 shows the

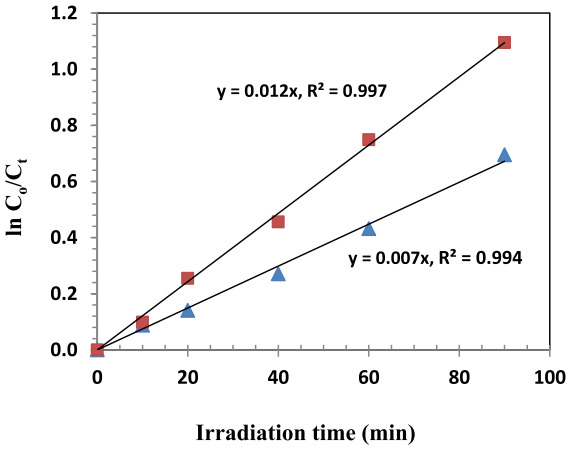

Figure 8. First-order kinetics plot for the photodegradation reaction of PCP with TiO_2 and Cr−TiO_2 (blue triangle up solid TiO_2 and brown box solid Cr−TiO_2).

variation of $\ln(C_0/C_t)$ as a function of irradiation time for TiO_2 and Cr−TiO_2. The plots demonstrated are all straight lines with $R^2 > 0.99$, which implies that the photocatalytic degradation strongly follows pseudo-first-order kinetics.

The apparent rate constants, k, for pure TiO_2 and Cr−TiO_2 are obtained as 0.0075 and 0.0122 min^{-1}, respectively. The integrated form of the Langmuir−Hinshelwood equation (eq 9) below has also been employed to predict the photocatalytic degradation rates of our pollutant PCP.

$$C = C_0 \exp(-k_{app}t) \tag{9}$$

Here, k_{app} is the apparent rate constant. This nonlinear model (eq 9) has been solved by the least-squares fitting technique.[73−75] All the resultant plots, as shown in Figure 9, reveal some well-behaved exponential curves, which are also consistent with the types reported earlier by other inves-

Table 2. Comparison of the Photocatalytic Activity of TiO_2 and Cr-doped TiO_2 with Other Photocatalysts for the degradation of PCP

	experimental conditions				
photocatalysts	catalyst dose (g/L)	light source	irradiation time (min)	degradation (%)	refs
TiO_2/GO		xenon lamp	300	65.5	68
10% La/TiO_2		plasma discharge	180	99.0	69
Pt−TiO_2	0.4	UV	240	90	70
Pd−TiO_2	0.4	UV	240	75	70
Ag−TiO_2	0.5	UV	360	64	71
Ag−TiO_2/Fe_3O4	0.5	UV	360	82	71
TiO_2	2.0	solar light	480	35	72
TiO_2	2.0	UV	90	50.23 ± 3.12	present work
Cr−TiO_2	2.0	UV	90	66.51 ± 2.14	present work

https://doi.org/10.1021/acsomega.2c05107
ACS Omega 2023, 8, 1979−1988

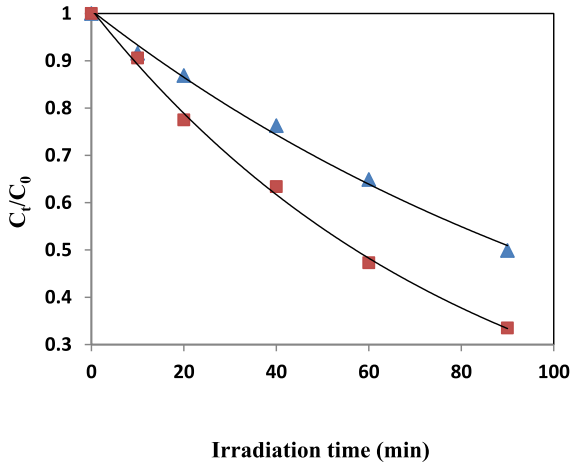

Figure 9. Change of C_t/C_0 with respect to irradiation time, at $[PCP]_0 = 1.0 \times 10^{-4}$ M and catalyst dose = 2.0 g/L (blue triangle up solid TiO_2 and red box solid $Cr-TiO_2$).

tigators.[74,76] However, in cases of both the linear and nonlinear methods, the photocatalytic data are thought to be in good fit with the pseudo-first-order approximation.

The NPs of $Cr-TiO_2$ show higher photocatalytic activity compared to the pure TiO_2, which is attributed as due to the introduction of Cr^{3+} ions into TiO_2 and that probably leads to an increment in its light absorption capacity. Furthermore, levels above the valence band maximum created by the Cr^{3+} ion doping can also trap the photogenerated holes, and hence resulting into the recombination suppression of electron–holes.[54]

Proposed Reaction Mechanism for the Photodegradation of PCP in Presence of TiO_2 and $Cr-TiO_2$. When light is exposed on the surface of the catalyst (TiO_2, $Cr-TiO_2$), an electron may transfer from the valence band to the conduction band, leaving a positive hole h^+ in the former. The probable reactions can be illustrated as below

$$TiO_2/Cr - TiO_2 + h\nu \rightarrow TiO_2/Cr - TiO_2(h^+ + e^-)$$

$$h^+ + H_2O \rightarrow {}^{\bullet}OH + H^+$$

$$e^- + O_2 \rightarrow O_2^{\bullet -}$$

$$PCP_{ads}{}^+ + ({}^{\bullet}OH,\ O_2^{\bullet})$$

$$\rightarrow \text{intermediate products}$$

$$\rightarrow \text{mineralized products}(CO_2,\ H_2O)$$

The free electrons then reduce the dissolved oxygen (O_2) into superoxide anion $O_2^{\bullet -}$ radicals, while the positive holes (h^+) react with the water generating $^{\bullet}OH$ radicals. These light-generated radicals through the formation of some intermediates are finally converting the PCP molecules into simple molecular units such as CO_2 and H_2O. From earlier studies the most typical intermediates created during the photocatalytic degradation of 4-CP are reported to be hydroquinones, hydroxyl hydroquinones, 4-chlororesorcinol, and 4-chlorocatechol.[6,77,78] Thus, based on the relevant reactions, Figure 10 schematically depicts the proposed mechanism for the photodegradation of PCP using TiO_2 and $Cr-TiO_2$ as the catalysts.

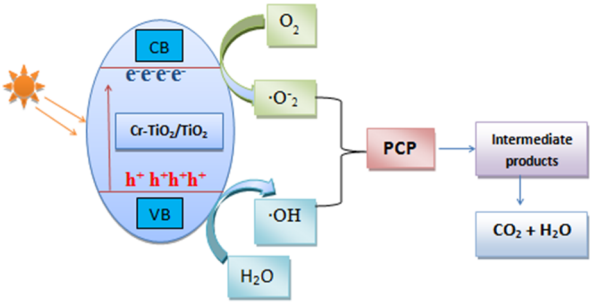

Figure 10. Schematic diagram of the proposed reaction mechanism for the photodegradation of PCP in presence of TiO_2 and $Cr-TiO_2$ NPs as catalysts.

CONCLUSIONS

Pure TiO_2 and Cr-doped TiO_2 were prepared successfully with a cost-effective and straightforward sol–gel method using TTIP as a precursor. Both NPs showed spherical-shaped anatase structures, and their crystalline sizes were 26.97 and 24.33 nm for pure TiO_2 and $Cr-TiO_2$, respectively. The EDS data confirmed that the formation of TiO_2 and $Cr-TiO_2$ were without any impurities. From the XPS analysis, for both types of NPs the Ti is found to be present as Ti^{4+} and Cr as Cr^{3+} in the $Cr-TiO_2$ samples.

The photocatalytic activity of the prepared TiO_2 and $Cr-TiO_2$ NPs was investigated for the degradation of PCP by varying the initial concentration of PCP, irradiation time, catalyst dosage, and pH. The optimal degradation capacity was observed for the initial concentration of PCP as $[PCP]_0 = 1.0 \times 10^{-4}$ M, catalyst dose as 2.0 g/L, and the irradiation time as 90 min, which is four times less than those reported earlier. Thus, the prepared $Cr-TiO_2$ NPs have enhanced the efficiency and reduced the irradiation time significantly. The photocatalytic degradation reaction of PCP is found to follow a pseudo-first-order kinetics, and the relevant rate constants are 0.0075 and 0.0122 min^{-1} for the pure TiO_2 and $Cr-TiO_2$, respectively. As a whole, within its shortest possible irradiation time the prepared Cr-doped TiO_2 NPs have also exhibited greater efficiency and higher degradation rate than that of pure TiO_2. Due to their excellent photocatalytic activity the $Cr-TiO_2$ NPs are therefore suggested to be used for degrading other organic pollutants as well.

ASSOCIATED CONTENT

Supporting Information

The Supporting Information is available free of charge at https://pubs.acs.org/doi/10.1021/acsomega.2c05107.

UV–vis spectra of PCP; atomic distribution; FTIR spectra; UV–vis spectra of PCP degradation; and degradation in the absence of catalyst and irradiation (PDF)

AUTHOR INFORMATION

Corresponding Author

Shamim Akhtar − *Department of Chemistry, University of Chittagong, Chittagong 4331, Bangladesh;* orcid.org/0000-0002-3398-4646; Email: ashamim@cu.ac.bd, shamim3332000@yahoo.com

https://doi.org/10.1021/acsomega.2c05107
ACS Omega 2023, 8, 1979−1988

Authors

Md. Kamrul Hossain − *Department of Chemistry, University of Chittagong, Chittagong 4331, Bangladesh*

Md. Mufazzal Hossain − *Department of Chemistry, University of Dhaka, Dhaka 1000, Bangladesh*

Complete contact information is available at: https://pubs.acs.org/10.1021/acsomega.2c05107

Notes

The authors declare no competing financial interest.

■ ACKNOWLEDGMENTS

The authors gratefully acknowledge the partial financial support from the University Grants Commission (UGC), Bangladesh.

■ REFERENCES

(1) Allaboun, H.; Al-Rub, F. A. A. Removal of 4-Chlorophenol from Contaminated Water Using Activated Carbon from Dried Date Pits: Equilibrium, Kinetics, and Thermodynamics Analyses. *Materials* **2016**, *9*, 251.

(2) Wang, M.; Fang, G.; Liu, P.; Zhou, D.; Ma, C.; Zhang, D.; Zhan, J. Fe_3O_4@β-CD nanocomposite as heterogeneous Fenton-like catalyst for enhanced degradation of 4-chlorophenol (4-CP). *Appl. Catal., B* **2016**, *188*, 113−122.

(3) Sharifi, Z.; Samadi, M. T.; Seid-Mohammadi, A.; Asgari, G. Removal of p-chlorophenol from aqueous solution using zerovalent-iron-based ultraviolet (UV/ZVI)/persulfate process. *J. Adv. Environ. Health Res.* **2016**, *4*, 42−48.

(4) Movahedyan, H.; Mohammadi, A. M. S.; Assadi, A. Comparison of different advanced oxidation processes degrading p-chlorophenol in aqueous solution. *Iran. J. Environ. Health Sci. Eng.* **2009**, *6*, 153−160.

(5) Sahinkaya, E.; Dilek, F. B. Biodegradation of 4-CP and 2,4-DCP mixture in a rotating biological contactor (RBC). *Biochem. Eng. J.* **2006**, *31*, 141−147.

(6) Hadi, S.; Taheri, E.; Amin, M. M.; Fatehizadeh, A.; Aminabhavi, T. M. Synergistic degradation of 4-chlorophenol by persulfate and oxalic acid mixture with heterogeneous Fenton like system for wastewater treatment: Adaptive neuro-fuzzy inference systems modeling. *J. Environ. Manage.* **2020**, *268*, 110678.

(7) Chen, J.; Sun, X.; Lin, L.; Dong, X.; He, Y. Adsorption removal of o-nitrophenol and p-nitrophenol from wastewater by metal-organic framework Cr-BDC. *Chin. J. Chem. Eng.* **2017**, *25*, 775−781.

(8) Suja, E.; Nancharaiah, Y. V.; Venugopalan, V. P. p-Nitrophenol biodegradation by aerobic microbial granules. *Appl. Biochem. Biotechnol.* **2012**, *167*, 1569−1577.

(9) Yin, C.; Cai, J.; Gao, L.; Yin, J.; Zhou, J. Highly efficient degradation of 4-nitrophenol over the catalyst of Mn_2O_3/AC by microwave catalytic oxidation degradation method. *J. Hazard. Mater.* **2016**, *305*, 15−20.

(10) Mahy, J. G.; Hermans, S.; Tilkin, D.; Lambert, S. D. Influence of nucleating agent addition on the textural and photo-Fenton properties of Fe(III)/SiO_2 catalysts. *J. Phys. Chem. Solids* **2020**, *144*, 109502.

(11) Belet, A.; Wolfs, C.; Mahy, J. G.; Poelman, D.; Vreuls, C.; Gillard, N.; Lambert, S. Sol-gel Syntheses of Photocatalysts for the Removal of Pharmaceutical Products in Water. *Nanomaterials* **2019**, *9*, 126.

(12) Yayapao, O.; Thongtem, T.; Phuruangrat, A.; Thongtem, S. Sonochemical synthesis of Dy-doped ZnO nanostructures and their photocatalytic properties. *J. Alloys Compd.* **2013**, *576*, 72−79.

(13) Yayapao, O.; Thongtem, T.; Phuruangrat, A.; Thongtem, S. Ultrasonic-assisted synthesis of Nd-doped ZnO for photocatalysis. *Mater. Lett.* **2013**, *90*, 83−86.

(14) Bavykina, A.; Kolobov, N.; Khan, S.; Bau, J. A.; Ramirez, A.; Gascon, J. Metal−Organic Frameworks in Heterogeneous Catalysis: Recent Progress. New Trends, and Future Perspectives. *Chem. Rev.* **2020**, *120*, 8468.

(15) Luo, H.; Gu, Y.; Liu, D.; Sun, Y. Advances in Oxidative Desulfurization of Fuel Oils over MOFs-Based Heterogeneous Catalysts. *Catalysts* **2021**, *11*, 1557.

(16) Dumrongrojthanath, P.; Thongtem, T.; Phuruangrat, A.; Thongtem, S. Synthesis and characterization of hierarchical multi-layered flower-like assemblies of Ag doped Bi_2WO_6 and their photocatalytic activities. *Superlattices Microstruct.* **2013**, *64*, 196−203.

(17) Phuruangrat, A.; Maneechote, A.; Dumrongrojthanath, P.; Ekthammathat, N.; Thongtem, S.; Thongtem, T. Effect of pH on visible-light-driven Bi2WO6 nanostructured catalyst synthesized by hydrotherma method. *Superlattices Microstruct.* **2015**, *78*, 106−115.

(18) Jraba, A.; Anna, Z.; Elaloui, E. Effects of Sr^{2+}, Fe^{3+} and Al^{3+} doping on the properties of TiO_2 prepared using the sol-gel method. *C. R. Chim.* **2019**, *22*, 648−658.

(19) Singh, A.; Kumar, S. Study of pure and Ag-doped TiO_2 nanoparticles for photocatalytic degradation of methylene blue. *IOP Conf. Ser.: Mater. Sci. Eng.* **2021**, *1033*, 012050.

(20) Rajaramanan, T.; Shanmugaratnam, S.; Gurunanthanan, V.; Yohi, S.; Velauthapillai, D.; Ravirajan, P.; Senthilnanthanan, M. Cost Effective Solvothermal Method to Synthesize Zn-doped TiO_2 Nanomaterials for Photovoltaic and Photocatalytic Degradation Applications. *Catalysts* **2021**, *11*, 690.

(21) Katta, K. V.; Dubey, R. S. Comparative study of doped-TiO_2 nanocrystals prepared by sol-gel and solvothermal approaches. *Mater. Today Proc.* **2021**, *39*, 1422−1425.

(22) Dubey, R. S.; Jadkar, S. R.; Bhorde, A. B. Synthesis and Characterization of Various Doped TiO_2Nanocrystals for Dye-Sensitized Solar Cells. *ACS Omega* **2021**, *6*, 3470−3482.

(23) Bharati, B.; Rath, C. Study of structural and magnetic properties of Mn-doped TiO2 nanoparticles. *AIP Conf. Proc.* **2018**, *1942*, 050134.

(24) Aqeel, M.; Ikram, M.; Imran, M.; Ul-Hamid, A.; Qumar, U.; Shahbaz, A.; Ikram, M.; Saeed, A. TiO_2 Co-doped with Zr and Ag shows highly efficient visible light photocatalytic behavior suitable for treatment of polluted water. *RSC Adv.* **2020**, *10*, 42235−42248.

(25) Zeng, X.; Sun, X.; Wang, Y. Photocatalytic degradation of flumequine by N-doped TiO_2 catalysts under simulated sunlight. *Environ. Eng. Res.* **2021**, *26*, 200524.

(26) Au-pree, S.; Narakaew, P.; Thungprasert, S.; Promanan, T.; Chaisena, A.; Narakaew, S. Enhanced Photocatalytic Activity of C-doped TiO_2 under Visible Light Irradiation: A Comparison of Corn Starch, Honey, and Polyethylene Glycol as a Carbon Sources. *Eng. J.* **2021**, *25*, 53−68.

(27) Zhang, Z.; Zhao, C.; Duan, Y.; Wang, C.; Zhao, Z.; Wang, H.; Gao, Y. Phosphorus-doped TiO_2 for visible-light-driven oxidative coupling of benzyl amines and photodegradation of phenol. *Appl. Surf. Sci.* **2020**, *527*, 146693.

(28) Zhu, M.; Zhai, C.; Qiu, L.; Lu, C.; Paton, A. S.; Du, Y.; Goh, M. C. New Method to Synthesize S-Doped TiO_2 with Stable and Highly Efficient Photocatalytic Performance under Indoor Sunlight Irradiation. *ACS Sustainable Chem. Eng.* **2015**, *3*, 3123−3129.

(29) Patehkhor, H. A.; Fattahi, M.; Khosravi-Nikou, M. Synthesis and characterization of ternary chitosan−TiO_2−ZnO over graphene for photocatalytic degradation of tetracycline from pharmaceutical wastewater. *Sci. Rep.* **2021**, *11*, 24177.

(30) Akhtar, J.; Tahir, M. B.; Sagir, M.; Bamufleh, H. S. Improved photocatalytic performance of Gd and Nd co-doped ZnO nanorods for the degradation of methylene blue. *Ceram. Int.* **2020**, *46*, 11955−11961.

(31) Prekajski, M.; Zarubica, A.; Babić, B.; Jokić, B.; Pantić, J.; Luković, J.; Matović, B. Synthesis and characterization of Cr^{3+} doped TiO_2 nanometric powders. *Ceram. Int.* **2016**, *42*, 1862−1869.

(32) Inturi, S. N. R.; Boningari, T.; Suidan, M.; Smirniotis, P. G. Visible-light-induced photodegradation of gas phase acetonitrile using aerosol-made transition metal (V, Cr, Fe, Co, Mn, Mo, Ni, Cu, Y, Ce, and Zr) doped TiO_2. *Appl. Catal., B* **2014**, *144*, 333−342.

(33) Ali, T.; Ahmed, A.; Alam, U.; Uddin, I.; Tripathi, P.; Muneer, M. Enhanced Photo- catalytic and antibacterial activities of Ag-doped TiO_2 nanoparticles under visible light. *Mater. Chem. Phys.* **2018**, *212*, 325−335.
(34) Dolatabadi, S.; Fattahi, M.; Nabati, M. Solid state dispersion and hydrothermal synthesis, characterization and evaluations of TiO_2/ZnO nanostructures for degradation of Rhodamine B. *Desalination Water Treat.* **2021**, *231*, 425−435.
(35) Dunnill, C. W.; Kafizas, A.; Parkin, I. P. CVD Production of Doped Titanium Dioxide Thin Films. Chemical Vapor Deposition. *Chem. Vap. Deposition* **2012**, *18*, 89−101.
(36) Asiltürk, M.; Sayılkan, F.; Arpaç, E. Effect of Fe^{3+} ion doping to TiO_2 on the photocatalytic degradation of Malachite Green dye under UV and vis irradiation. *J. Photochem. Photobiol.* **2009**, *203*, 64−71.
(37) Natarajan, T. S.; Natarajan, K.; Bajaj, H.; Tayade, R. Enhanced photocatalytic activity of bismuth-doped TiO_2 nanotubes under direct sunlight irradiation for degradation of Rhodamine B dye. *J. Nanopart. Res.* **2013**, *15*, 1−18.
(38) Yang, G.; Yan, Z.; Xiao, T. Low-temperature solvothermal synthesis of visible light-responsive S-doped TiO_2 nanocrystal. *Appl. Surf. Sci.* **2012**, *258*, 4016−4022.
(39) Byun, D.; Jin, Y.; Kim, B.; Lee, J. K.; Park, D. Photocatalytic TiO_2 deposition by chemical vapor deposition. *J. Hazard. Mater. B* **2000**, *73*, 199−206.
(40) Haque, F. Z.; Nandanwar, R.; Singh, P. Evaluating photo-degradation properties of anatase and rutile TiO_2 nanoparticles for organic compounds. *Optik* **2017**, *128*, 191−200.
(41) Feng, W.; Mu-sen, L. M.; Yu-peng, L. Y.; Yong-xin, Q. Y. A simple sol-gel technique for preparing Hydroxyapatite nanopowders. *Mater. Lett.* **2005**, *59*, 916−919.
(42) Oskam, G.; Nellore, A.; Penn, R. L.; Searson, P. C. The growth kinetics of TiO_2 nanoparticles from titanium (IV) alkoxide at high water/titanium ratio. *J. Phys. Chem. B* **2003**, *107*, 1734.
(43) Mendiola-Alvarez, S. Y.; Guzmán-Mar, J. L.; Turnes-Palomino, G.; Maya-Alejandro, F.; Caballero-Quintero, A.; Hernández-Ramírez, A.; Hinojosa-Reyes, L. Synthesis of Cr^{3+}-doped TiO_2 nanoparticles: Characterization and evaluation of their visible photocatalytic performance and stability. *Environ. Technol.* **2019**, *40*, 144−153.
(44) Hamadanian, M.; Sarabi, A. S.; Mohammadi Mehra, A. M.; Jabbari, V. Photocatalyst Cr-doped titanium oxide nanoparticles: Fabrication, characterization, and investigation of the effect of doping on methyl orange dye degradation. *Mater. Sci. Semicond. Process.* **2014**, *21*, 161−166.
(45) Hasan, A. H.; Hasan, F. Synthesis of Cr Doped TiO_2 Using Sol-Gel Technique and Calculation of its Photocatalytic Activity. *Indian J. Nat. Sci.* **2019**, *9*, 15242−15259.
(46) Dubey, R. S.; Singh, S. Investigation of structural and optical properties of pure and chromium doped TiO_2 nanoparticles prepared by solvothermal method. *Results Phys.* **2017**, *7*, 1283−1288.
(47) Khairy, M.; Zakaria, W. Effect of metal-doping of TiO_2 nanoparticles on their photocatalytic activities toward removal of organic dyes. *Egypt. J. Pet.* **2014**, *23*, 419−426.
(48) Wu, J. C. S.; Lin, H. M. Photoreduction of CO_2 to methanol via TiO_2 photocatalyst. *Int. J. Photoenergy* **2005**, *7*, 115−119.
(49) Razali, M. H.; Mohamed, A. R.; Sreekantan, S. Morphological, Structural and Optical Properties Study of Transition Metal Ions Doped TiO_2 Nanotubes Prepared by Hydrothermal Method. *Int. J. Mater. Mech. Manuf.* **2013**, *1*, 314−318.
(50) Khlyustova, A.; Sirotkin, N.; Kusova, T.; Kraev, A.; Titov, V.; Agafonov, A. Doped TiO_2: The effect of doping elements on photocatalytic activity. *Mater. Adv.* **2020**, *1*, 1193−1201.
(51) Zhu, X.; Pei, L.; Zhu, R.; Jiao, Y.; Tang, R.; Feng, W. Preparation and characterization of Sn/La co-doped TiO_2 nanomaterials and their phase transformation and photocatalytic activity. *Sci. Rep.* **2018**, *8*, 12387.
(52) Chen, C.; Lei, X. F.; Xue, M. Z. A simple method to synthesize Ag-doped TiO_2 photocatalysts with different AgO: Ag_2O atomic ratios for enhancing visible-light photocatalytic activity. *J. Chem. Res.* **2017**, *41*, 475−483.
(53) Akshay, V. R.; Arun, B.; Mandal, G.; Vasundhara, M. Visible range optical absorption, Urbach energy estimation and paramagnetic response in Cr-doped TiO_2nanocrystals derived by a sol-gel method. *Phys. Chem. Chem. Phys.* **2019**, *21*, 12991.
(54) Li, X.; Zhengkai, G.; Tao, H. The doping mechanism of Cr into TiO_2 and its influence on the photocatalytic performance. *Phys. Chem. Chem. Phys.* **2013**, *15*, 20037.
(55) Tian, B.; Li, C.; Zhang, J. One-step preparation, characterization and visible-light photocatalytic activity of Cr-doped TiO_2 with anatase and rutile bicrystalline phases. *Chem. Eng. J.* **2012**, *191*, 402−409.
(56) Zielińska, A.; Kowalska, E.; Sobczak, J. W.; Lacka, I.; Gazda, M.; Ohtani, B.; Hupka, J.; Zaleska, A. Silver-doped TiO_2 prepared by microemulsion method: surface properties, bio- and photoactivity. *Sep. Purif. Technol.* **2010**, *72*, 309−318.
(57) Fan, X.; Fan, J.; Hu, X.; Liu, E.; Kang, L.; Tang, C.; Ma, Y.; Wu, H.; Li, Y. Preparation and characterization of Ag deposited and Fe doped TiO_2 nanotube arrays for photocatalytic hydrogen production by water splitting. *Ceram. Int.* **2014**, *40*, 15907−15917.
(58) Jia, T.; Fu, F.; Yu, D.; Cao, J.; Sun, G. Facile synthesis and characterization of N-doped TiO_2/C nanocomposites with enhanced visible-light photocatalytic performance. *Appl. Surf. Sci.* **2018**, *430*, 438−447.
(59) MirzaHedayat, B.; Noorisepehr, M.; Dehghanifard, E.; Esrafili, A.; Norozi, R. Evaluation of photocatalytic degradation of 2, 4-Dinitrophenol from synthetic wastewater using Fe_3O_4 @SiO_2@TiO_2/rGO magnetic nanoparticles. *J. Mol. Liq.* **2018**, *264*, 571−578.
(60) Ali, M. H. H.; Al-Qahtani, K. M.; El-Sayed, S. M. Enhancing photodegradation of 2,4,6 trichlorophenol and organic pollutants in industrial effluents using nanocomposite of TiO_2 doped with reduced graphene oxide. *Egypt. J. Aquat. Res.* **2019**, *45*, 321−328.
(61) Neppolian, B.; Choi, H. C.; Sakthivel, S.; Arabindoo, B.; Murugesan, V. Solar/UV-induced photocatalytic degradation of three commercial textile dyes. *J. Hazard. Mater.* **2002**, *89*, 303.
(62) Dixit, A.; Mungray, A.; Chakraborty, M. Photochemical oxidation of phenol and chlorophenol by UV/H_2O_2/TiO_2 process: a kinetic study. *Int. J. Chem. Eng. Appl.* **2010**, *1*, 247.
(63) Venkatachalam, N.; Palanichamy, M.; Murugesan, V. Sol-gel preparation and characterization of alkaline earth metal doped nano TiO_2: Efficient photocatalytic degradation of 4-chlorophenol. *J. Mol. Catal. A: Chem.* **2007**, *273*, 177−185.
(64) Hadi, S.; Taheri, E.; Amin, M. M.; Fatehizadeh, A.; Aminabhavi, T. M. Synergistic degradation of 4-chlorophenol by persulfate and oxalic acid mixture with heterogeneous Fenton like system for wastewater treatment: Adaptive neuro-fuzzy inference systems modeling. *J. Environ. Manage.* **2020**, *268*, 110678.
(65) Kantar, C.; Oral, O.; Urken, O.; Oz, N. A.; Keskin, S. Oxidative degradation of chlorophenolic compounds with pyrite-Fenton process. *Environ. Pollut.* **2019**, *247*, 349−361.
(66) Ahmed, S.; Rasul, M. G.; Martens, W. N.; Brown, R.; Hashib, M. A. Heterogeneous photocatalytic degradation of phenols in wastewater: A review on current status and developments. *Desalination* **2010**, *261*, 3−18.
(67) Okamoto, K.; Yamamoto, Y.; Tanaka, H.; Tanaka, M.; Itaya, A. Heterogeneous photocatalytic decomposition of phenol over TiO_2 powder. *Bull. Chem. Soc. Jpn.* **1985**, *58*, 2015−2022.
(68) Xu, Z.; Zhang, J.; Liu, H.; Kuang, P.; Wang, S.; Fu, X. Preparation of silver/silver bromide/titanium dioxide/graphene oxide nanocomposite for photocatalytic degradation of 4-chlorophenol. *Nanomater. Nanotechnol.* **2017**, *7*, 1−8.
(69) Li, S.; Xu, Y.; Wang, X.; Guo, Y.; Mu, Q. Catalytic degradation of 4-chlorophenol with La/TiO2 in dielectric barrier discharge system. *RSC Adv.* **2016**, *6*, 28994−29002.
(70) Kim, K.; Ha, H. J.; Lee, S. K.; Lee, J. K. Degradation of Chlorophenol by Photocatalysts with Various Transition Metals. *Korean J. Chem. Eng.* **2005**, *22*, 382−386.
(71) Chang, S. W.; Chung, W. J.; Yu, S. H.; Lee, S. J. Photocatalytic degradation of 4-chlorophenol using a Ag/TiO_2/Fe_3O_4 composite

https://doi.org/10.1021/acsomega.2c05107
ACS Omega 2023, 8, 1979−1988

under UV-A irradiation. *Desalination Water Treat.* **2015**, *54*, 3646−3653.
(72) Payan, A.; Fattahi, M.; Roozbehani, B.; Jorfi, S. Enhancing Photocatalytic Activity of Nitrogen Doped TiO_2 for Degradation of 4-Chlorophenol under Solar Light Irradiation. *Iran. J. Chem. Eng.* **2018**, *15*, 3−14.
(73) Perrin, C. L. Linear or nonlinear least-squares analysis of kinetic data. *J. Chem. Educ.* **2017**, *94*, 669−672.
(74) Lente, G. Facts and alternative facts in chemical kinetics: remarks about the kinetic use of activities, termolecular processes, and linearization techniques. *Curr. Opin. Chem. Eng.* **2018**, *21*, 76−83.
(75) Lente, G.*Deterministic kinetics in chemistry and systems biology: the dynamics of complex reaction networks*; Springer; New York, 2015.
(76) Yusuff, A. S.; Bello, K. A.; Azeez, T. M. Photocatalytic degradation of an anionic dye in aqueous solution by visible light responsive zinc oxide-termite hill composite. *React. Kinet., Mech. Catal.* **2020**, *131*, 537−554.
(77) Duan, F.; Yang, Y.; Li, Y.; Cao, H.; Wang, Y.; Zhang, Y. Heterogeneous Fenton-like degradation of 4-chlorophenol using iron/ordered mesoporous carbon catalyst. *J. Environ. Sci.* **2014**, *26*, 1171−1179.
(78) Selvam, N. C. S.; Narayanan, S.; Kennedy, L. J.; Vijaya, J. J. Pure and Mg-doped self-assembled ZnO nano-particles for the enhanced photocatalytic degradation of 4-chlorophenol. *J. Environ. Sci.* **2013**, *25*, 2157−2167.

https://doi.org/10.1021/acsomega.2c05107
ACS Omega 2023, 8, 1979−1988